sustainability

MDPI

Article

Analyzing Water and Sediment Flow Patterns in Circular Forebays of Sediment-Laden Rivers

Haidong Wang [1], Yuji Tai [2], Lingxiao Huang [3,*], Cheng Yang [4] and Hefang Jing [4]

1 College of Civil and Hydraulic Engineering, Ningxia University, Yinchuan 750021, China; haidongwang626@stu.nxu.edu.cn
2 Civil Engineering & Architecture, Anhui University of Technology, Ma'anshan 243002, China; taiyj@hnu.edu.cn
3 College of Information Engineering, Ningxia University, Yinchuan 750021, China
4 College of Civil Engineering, North Minzu University, Yinchuan 750021, China; yang_cheng@nun.edu.cn (C.Y.); jinghef@163.com (H.J.)
* Correspondence: huanglx@nxu.edu.cn

Abstract: In the circular forebay of sediment-laden rivers, adverse flow patterns such as vortices emerge, leading to substantial sediment accumulation along the sidewalls of the diversion channel and in the forebay. This sediment accumulation significantly impacts the operational efficiency of water pumps. To address these challenges, a combination of numerical simulations and engineering experiments was employed to reveal the factors contributing to the development of these patterns. Based on these findings, seven distinct flow rates and operating conditions were introduced to obtain the optimal inlet flow rate and increase the sustainability of engineering use. The findings revealed that the different inlet flow rates exert varying influences on the flow patterns in the circular forebay, leading to changes in sediment levels in both the forebay and diversion channels. Following comprehensive comparison, Scheme 6 was identified as the optimal flow rate scheme. In this scheme, the flow uniformity, deviation angle, ratio of the vortex reduction area parameter, and rate of vortex area reduction in sections z1−3 were markedly enhanced. The effectiveness of this scheme was validated through rigorous numerical simulations and engineering experiments, thereby offering indispensable theoretical insights into the operation of pumping stations in circular forebays.

Keywords: sediment-laden rivers; circular forebay; vortex flow pattern; numerical simulations; optimal scheme

check for updates

Citation: Wang, H.; Tai, Y.; Huang, L.; Yang, C.; Jing, H. Analyzing Water and Sediment Flow Patterns in Circular Forebays of Sediment-Laden Rivers. *Sustainability* **2023**, *15*, 16941. https://doi.org/10.3390/su152416941

Received: 11 October 2023
Revised: 29 November 2023
Accepted: 14 December 2023
Published: 18 December 2023

Copyright: © 2023 by the authors. Licensee MDPI, Basel, Switzerland. This article is an open access article distributed under the terms and conditions of the Creative Commons Attribution (CC BY) license (https://creativecommons.org/licenses/by/4.0/).

1. Introduction

Due to its distinctive geographical location, the northwest region faces formidable challenges related to water scarcity [1]. In addressing this issue, pumping stations assume a pivotal role in water resource management in China [2]. These stations not only facilitate efficient water irrigation but also significantly contribute to flood control, drainage, and the provision of essential domestic water for residents [3]. Nevertheless, due to various factors, most forebays exhibit suboptimal flow patterns, characterized by countercurrents and vortices [4]. These issues not only deteriorate the inlet conditions of pumping stations but also generate adverse consequences such as sediment accumulation, equipment vibrations, and noise, all of which significantly impair the operational efficiency of pumping stations. Therefore, it becomes imperative to implement judicious measures to address flow pattern concerns in the forebay and minimize sediment accumulation [5]. The ultimate aim of these measures is to optimize forebay flow patterns, increase the sustainability of engineering use, and inhibit the occurrence of countercurrents and vortices while effectively mitigating sediment deposition [6].

Against the backdrop of ongoing advancements in computational fluid dynamics and turbulence models [7], the utilization of the numerical simulation method for analyzing flow patterns in pumping station forebays [8] has yielded significant practical implications. The application of this method has laid a critical theoretical foundation for pumping station engineering [9]. Through the use of numerical simulations [10], we could comprehensively obtain the flow dynamics in the forebay [11]. Furthermore, this approach could enable us to anticipate issues such as countercurrents and vortices, thus offering dependable insights for both the design and enhancement of pumping stations [12]. Moreover, numerical simulation analysis can reveal intricate flow characteristics [13]; for example, Nasr [14] meticulously examined and compared various rectification methodologies. Employing numerical simulations, they identified a remedial approach tailored to the front pool of the lateral inlet pump station. This approach yielded an 8% enhancement in the uniformity of the flow velocity in the front pool, as well as an impressive 70% reduction in the vortex area. By employing the image velocimetry technique, Xi and Lu [15] acquired flow field data from both the front and inlet tanks of the pump station, subsequently substantiating these data through comprehensive numerical simulations. This research findings notably revealed an asymmetrical nature of the inlet vorticity in the forebay of the lateral pumping station. This asymmetry, in turn, induced an irregular distribution of inlet water, thereby triggering perturbations in flow dynamics and subsequently causing vibrations and disruptions in the pumping unit. These findings unequivocally indicate a notable threat to overall engineering safety. Regarding the analysis of the pump station forebay, Tang [16] applied the lattice Boltzmann method (LBM) coupled with the subgrid stress (SGS) model and predicted the secondary flow and water level characteristics in the forebay. Through changes in geometric parameters, Xu [17] analyzed a shrinkage diversion pier. When this type of diversion pier is located in the middle of the reflux area, the flow pattern in the inlet pool could be appropriately improved to optimize the inlet conditions of the pump station.

In recent years, propelled by ongoing advancements in remote sensing technology and numerical modeling [18], remarkable advances have been accomplished in river sediment dynamics research [19]. Budinski and Spasojević [20] introduced the control equation and the corresponding numerical solution in a comprehensive nonorthogonal curvilinear coordinate system. This study was executed using a detailed, step-by-step numerical solution approach. The high-order interpolation feature method was seamlessly integrated, considering both the detection of flow and suspended sediment. Through the comparison of the numerical simulation results with real-world measurements, the approach of incorporating sediment mixtures into the flow sediment model was favorably substantiated. Serra [21] employed hysteresis loops as a means to determine and draw comparisons regarding the transport of suspended sediment with distinct particle sizes during river floods. It was observed that particles of varying sizes are transported in diverse manners under identical water flow conditions. Concurrently, controlled artificial floods could be strategically employed for river restoration purposes. Yuan [22] proposed a new sediment feeder for loading dry sediment samples at the inlet as well as a pressurized sediment filter for screening sediment at the outlet to achieve a clean water supply system for the water tank suitable for simulating the transport of fine-grained pollutants in low-sediment-concentration river turbulence.

Based on the above summary, most of the current research on forebays has focused on clear water experiments, with few studies on the two-phase flow of water and sand in forebays, and there is almost no research on the flow state of circular forebays. Therefore, the main objective of this article is to conduct in-depth research on the flow characteristics and sedimentation problems of circular forebays to increase the sustainability of the use of circular pumping station engineering. Through this exhaustive exploration, our primary objective was to examine and obtain an empirically derived and appropriately validated inlet flow rate specific to circular forebays. This effort could encompass comprehensive optimization of the intrinsic flow patterns in circular forebays, with a parallel focus on addressing the challenges of sediment deposition. The outcomes of this study could offer substantial and sound guidance for the intricate design and engineering configuration of circular forebays in the broader domain of pump station infrastructure.

2. Research Area, Data, and Methods

2.1. Research Area

This study conducts a comprehensive investigation and analytical assessment of multiple circular pumping station forebays in Gansu Province, China, as illustrated in Figure 1. When the water flows into two circular forebays from the Y-shaped diversion channel, the diversion channel forks at the end. Due to the diversion, the flow velocity tends to increase on the outer side and decrease on the inner side. The uneven flow velocity causes backflow at the connection between the diversion channel and the forebay. When the main flow enters the circular forebay from the channel, the water flows directly into the bottom from the middle, resulting in significant backflow on both sides of the forebay, which is affected by the channel flow velocity. The outer recirculation zone is larger than the inner recirculation zone, and at the same time, the water flow will form a vertical rotation and roll under the water surface, forming a water-carrying sediment movement. The disordered flow pattern will inevitably affect the efficiency of the pumping station, and all the sediment accumulation in the circular forebay is at the bottom of the pool, making dredging work relatively more difficult. The existing working conditions do not have a significant sustainable effect on the circular pumping station forebay project.

The principal quandaries encountered within these circular forebays are as follows:

1. Vortex formation and nonuniform flow: Within the circular forebays, fluid dynamics give rise to vortices and eddies. These intricate hydrodynamic phenomena can induce nonuniform flow profiles, notably affecting the inlet dynamics of the pump station and the operational efficacy of associated machinery.
2. Sediment accumulation: Gansu Province's geographical positioning within the middle and upper reaches of the Yellow River exposes it to a risk of heightened sediment content. This can lead to the ingress of considerable sediment loads from canal waters into circular forebays. In regions characterized by diminished flow velocities within circular forebays, sediment particulates tend to deposit along the substrate and sidewalls, leading to sedimentary deposition.
3. Uneven horizontal distribution and flow velocity distribution: The prevailing heterogeneities in horizontal and flow velocity distributions indigenous to circular forebays have the potential to induce perturbations in inlet stability, leading to measurable reductions in pump station operational efficiency. These nonuniformities can be attributed to an intricate interplay of factors encompassing inlet flow rates, basin geomorphology, and sidewall configurations.
4. Temporal fluctuations in water elevation and pressure gradients: The temporal oscillations in water elevation and concomitant pressure gradients within circular forebays have a pronounced influence on the operational modalities and inlet conditions of pumping stations. Misaligned water level dynamics and pressure gradients can present challenges ranging from flow instabilities to hydraulic perturbations.

After assessing numerous circular forebays, this study selects representative circular forebays for analysis. Notably, this specific collection of forebays presents intricate challenges characterized by the emergence of vortex-induced flow patterns and the consequential predicament of sediment accumulation, significantly complicating the execution of dredging operations. In light of these intricate dynamics, this study examines flow rate modulation at the ingresses of circular forebays.

2.2. Research Data and Calculation Methods

2.2.1. Research Data

According to the measurement data of water volume and sediment inflow near the Yellow River Basin diversion channel in the past eight years (2015–2022), these data were drawn by our research team through years of monitoring and statistics, as shown in Table 1. Our analysis reveals that the predominant catalyst for sediment accumulation within the pump station's anterior pool is the pronounced sediment concentration in the diversion channel. Sediment concentrations are notably elevated from July to October. Consequently, to conduct a more comprehensive inquiry, we adopted an average sediment content of "2.62 kg/m^3" for these four months. This simulation, spanning a duration of 110 days, is undertaken to thoroughly scrutinize and analyze shifts in sediment content and flow patterns within the forebay across varying flow velocities.

(**a**) Vortex flow pattern (**b**) Sedimentation

(**c**) Dredging operation

Figure 1. Potential problems in a circular forebay.

Table 1. Statistical analysis of monthly average water and sediment characteristics from 2015 to 2022.

Project	Month												Annual
	1	2	3	4	5	6	7	8	9	10	11	12	
Water volume (B m^3)	1.62	1.651	1.726	1.899	1.912	2.098	2.152	2.998	3.102	2.935	1.536	1.498	25.127
Sediment (M kg)	48.15	37.42	158.63	392.41	1149.56	1432.12	4563.32	11,204.13	5736.45	8213.65	283.61	145.56	33,365.01
Sediment concentration (kg/m^3)	0.029	0.023	0.092	0.207	0.601	0.683	2.121	3.737	1.849	2.799	0.185	0.097	1.328

2.2.2. Control Equation

The selection of the mixture model for addressing the two-phase flow intricacies within the circular forebay is based on the following factors:

1. The mixture model [23] can proficiently capture the intricacies of solid-fluid coupling in water and sand two-phase flow within circular forebays. Accounting for interactions and mutual influences between the water and sand phases significantly enhances the precision of simulation outcomes.

2. The mixture model [24] can seamlessly accommodate scenarios involving mixed water–sand flow within diversion channels, characterized by incompressible fluid dynamics. This adaptability ensures the fidelity and accuracy of simulations.
3. The mixture model [25] demonstrates a credible alignment with the complexities of sediment distribution, vortex formation, and the behavior of low-load particles within circular forebays. It can adeptly consider factors such as momentum continuity, relative velocities, and volume fractions of distinct particles, thereby providing a more accurate portrayal of mixture motion characteristics.
4. The algebraic expressions intrinsic to the mixture model can be effectively solved and simulated through numerical methodologies. This feature streamlines the computational process and facilitates the comprehensive analysis of dynamic attributes in water and sediment two-phase flow within circular forebays.

In summary, to address a two-phase flow problem in a circular forebay, the mixture model was selected to provide a powerful tool for in-depth analysis and simulation of water sediment two-phase flow. The mathematical expression [26] is provided as follows:

In the circular forebay, the above formulas can be explained as follows: The continuity equation and momentum equation of two-phase flow can be expressed as Equations (1) and (2), where the average velocity of mass $\overrightarrow{v_m}$ represents the average velocity of the water and sediment phases, ρ_m represents the density of the water–sand mixture, α_k represents the volume fraction of the k-th phase, n represents the number of phases, $\vec{F}$ represents the volume force, and μ_m represents the viscosity of the mixture.

$$\frac{\partial}{\partial t}(\rho_m) + \nabla\cdot\left(\rho_m \overrightarrow{v_m}\right) = 0 \tag{1}$$

$$\frac{\partial}{\partial t}\left(\rho_m \overrightarrow{v_m}\right) + \nabla\cdot\left(\rho_m \overrightarrow{v_m}\,\overrightarrow{v_m}\right) = -\nabla p + \nabla\cdot\left[\mu_m\left(\nabla\overrightarrow{v_m} + \nabla\overrightarrow{v_m}^T\right)\right] + \rho_m \vec{g} + \vec{F} - \nabla\cdot\left(\sum_{k=1}^{n} \alpha_k \rho_k \overrightarrow{v_{dr,k}}\,\overrightarrow{v_{dr,k}}\right) \tag{2}$$

The drift velocity $\overrightarrow{v_{dr,k}}$ in Equation (2) is represented as the sediment velocity of the second phase sediment, and $\overrightarrow{v_{dr,k}}$ can be defined using Equation (3).

$$\overrightarrow{v_{dr,k}} = \overrightarrow{v_k} - \overrightarrow{v_m} \tag{3}$$

The relationship between drift velocity and relative velocity can be expressed by Equation (4), where relative velocity $\overrightarrow{v_{pq}}$ represents the velocity of the secondary phase (sediment "p") relative to the main phase (water "q").

$$\overrightarrow{v_{dr,p}} = \overrightarrow{v_{pq}} - \sum\nolimits_{k=1}^{n} \frac{\alpha_k \rho_k}{\rho_m} \overrightarrow{v_{kq}} \tag{4}$$

$$\overrightarrow{v_{pq}} = \overrightarrow{v_p} - \overrightarrow{v_q} \tag{5}$$

The mass fractions of the water and sand phases can be defined using Equation (6).

$$C_k = \frac{\alpha_k \rho_k}{\rho_m} \tag{6}$$

Based on Equations (1)–(6), the volume fraction of the sediment phase can be expressed as Equation (7).

$$\frac{\partial}{\partial_t}(\alpha_p \rho_p) + \nabla\cdot(\alpha_p \rho_p \overrightarrow{v_m}) = -\nabla(\alpha_p \rho_p \overrightarrow{v_{dr,p}}) + \sum\nolimits_{q=1}^{n}(\dot{m}_{qp} - \dot{m}_{pq}) \tag{7}$$

2.3. Reynolds Equation, Grid Division, and Boundary Conditions

2.3.1. Reynolds Equation

At present, the commonly used model for the numerical simulation of flow patterns in the forebays of pumping stations is the $k-\varepsilon$ [27] model. Turbulent viscosity is determined by the turbulent kinetic energy [28] of k and the turbulent dissipation rate [29] ε calculated using the transport equation. Perform a 1:1 restoration model based on the actual size of the circular forebay. This study selected five cross-sections within the circular forebay, located at distances of 2 m and 8 m from the diversion canal mouth and 6.8 m, 11.80 m, and 14.7 m from point A, labeled Y1, Y2, Y3-1, Y3-2, Y4-1, Y4-2, Y5-1, and Y5-2, respectively, as shown in Figure 2. On cross-sections Y1, Y2, Y3, and Y4, flow velocity monitoring points with a depth of 2 m were set up. On cross-sections Y4 and Y5, flow velocity monitoring points with a depth of 3 m were set up, with a spacing of 0.2 m between monitoring points. The numerical simulations were conducted using standard $k-\varepsilon$ [30] models, RNG $k-\varepsilon$ [31] models, and realizable $k-\varepsilon$ [32] models. As shown in Figure 3, we compare and analyze the flow velocity between the measured data and the simulation results of each model. The flow velocity value is taken from the average flow velocity from June to September at the monitoring point. There is no proof of which is more suitable for the turbulence model of the pump station forebay, and research and demonstration can only be conducted through measured results and numerical simulation results. The results show that the standard $k-\varepsilon$ model are close to the measured data, so this study chose this model to improve the flow state in the forebay of the pump station.

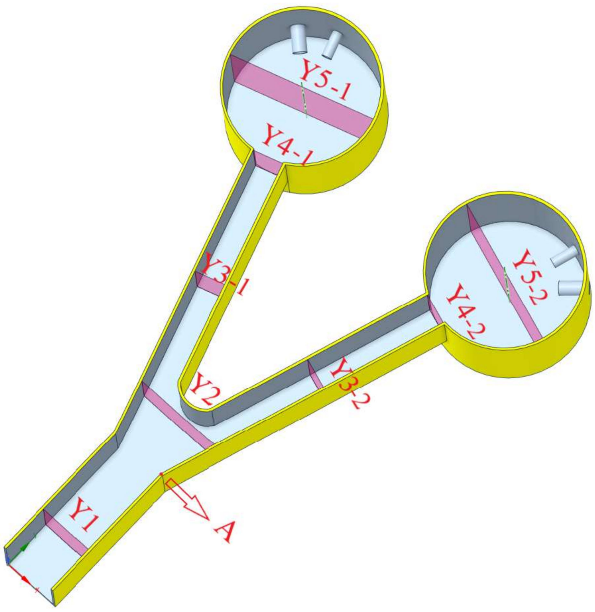

Figure 2. Cross-section velocity distribution. Point A is the diversion point between the linear and Y-shaped diversion channels.

2.3.2. Mesh Generation

To improve the reliability of the numerical simulation results and reduce the computational workload, in the circular forebay, the solid region is suppressed and only the fluid part is calculated, as shown in Figure 4, to distinguish between the solid wall and the fluid region. Therefore, unstructured mesh partitioning was performed on the fluid region of the circular forebay. The grid inside the circular forebay is divided into four areas: the inlet area, the diversion channel and forebay area, and the pump station outlet area. Local grid refinement is performed in the inlet and outlet areas.

Due to the complexity of the boundary conditions of the circular forebay and the presence of pumping pipes [33] in the outlet area, as well as the significant impact of the quantity and quality of the grids on the numerical calculation results [34], the grids were divided into 8 groups in the irrelevance analysis, with quantities of 280,000, 470,000, 660,000, 820,000, 1.03 million, 1.25 million, 1.67 million, and 1.99 million. According to the formula:

$$H_f = \frac{(v_{in}^2 - v_{out}^2)}{2g} + \frac{(P_{in} - P_{out})}{\rho g} + (Z_{in} - Z_{out}) \tag{8}$$

The hydraulic loss H_f and pump efficiency η from inlet to outlet in the calculation domain were selected as the objective functions and verified [35]. In Equation (8), v_{in} is the mixed flow velocity of water and sediment at the inlet of the circular forebay, v_{out} is the mixed flow velocity of water and sediment at 0.2 m in front of the pumping pipes of the four pumps in the circular forebay, and v_{in} and v_{out} are the average of the absolute values of the mixed flow velocity of water and sediment. P_{in} and P_{out} are the inlet and outlet pressures of the circular forebay, where they are considered static pressure; Z_{in} and Z_{out} are the inlet and outlet potential energies of the circular forebay. As shown in Figure 5, the results show that when the number of grids increases to 1.67 million, the error is within 2.0%, indicating that the model has passed the grid independence test. In the circular forebay model, a total of 1,677,326 grids were ultimately divided, as shown in Figure 6. To ensure computational accuracy, a second-order upwind plane implicit solution was used for the fluid domain in the circular forebay, and the semi-implicit method of pressure link equation consistency (SIMPLEC) algorithm was used for flow field coupling. Meanwhile, the finite volume method was used for computational analysis of the entire fluid domain.

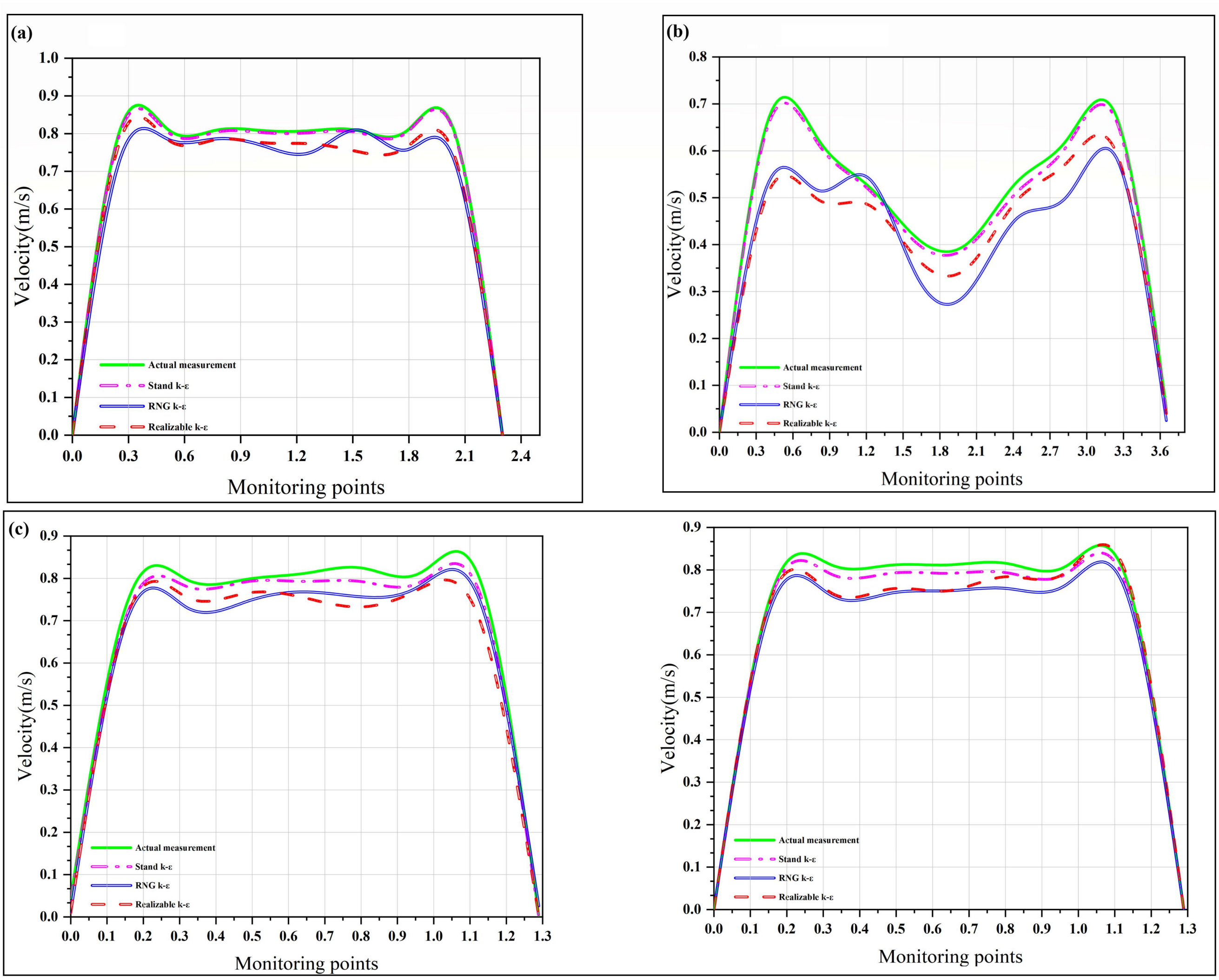

Figure 3. *Cont.*

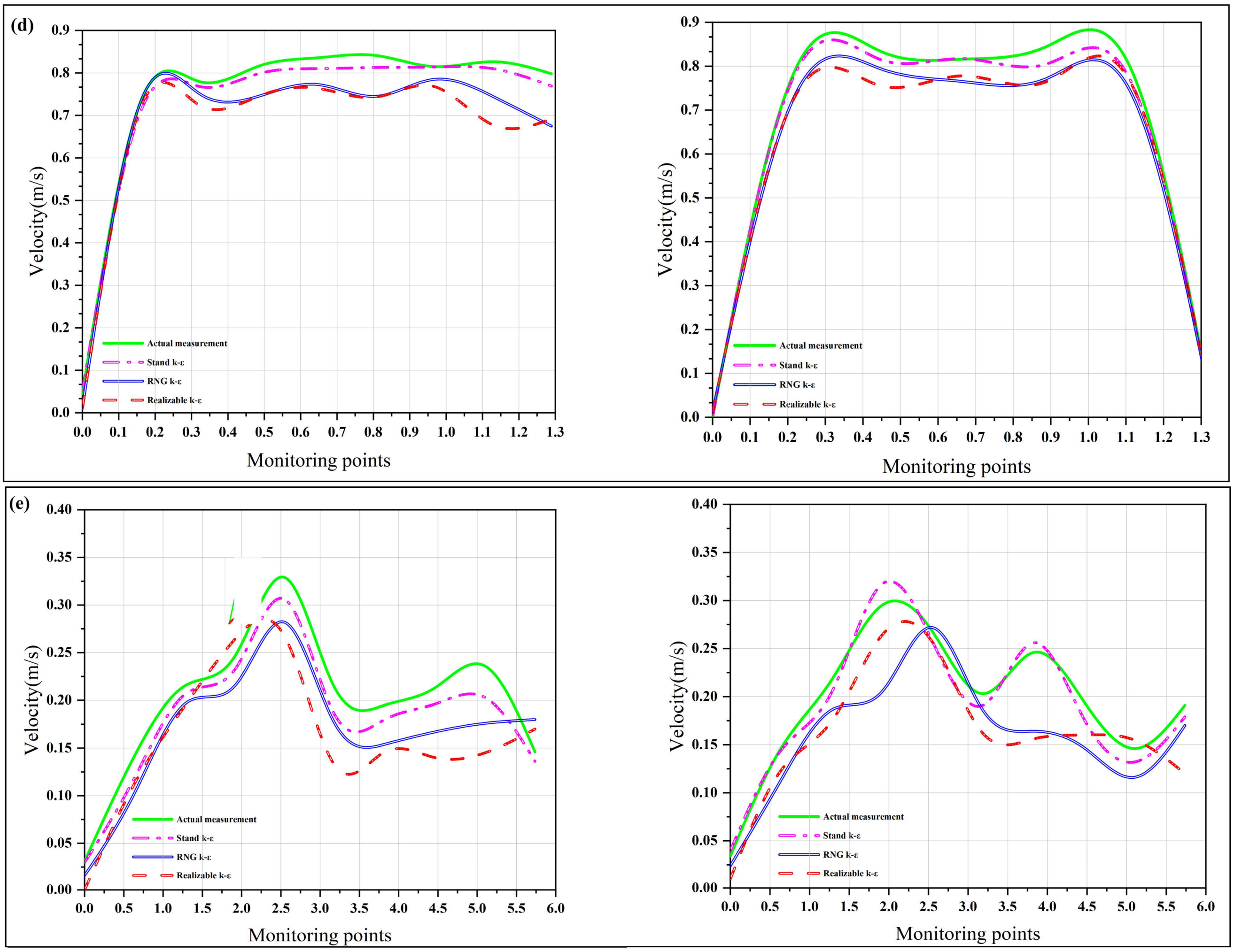

Figure 3. Comparison of flow velocity between various turbulence models and measured flow. (**a**) Comparison of flow velocity at the Y1 section. (**b**) Comparison of flow velocity at the Y2 section. (**c**) Comparison of flow velocity at the Y3 section. (**d**) Comparison of flow velocity at the Y4 section. (**e**) Comparison of flow velocity at the Y5 section.

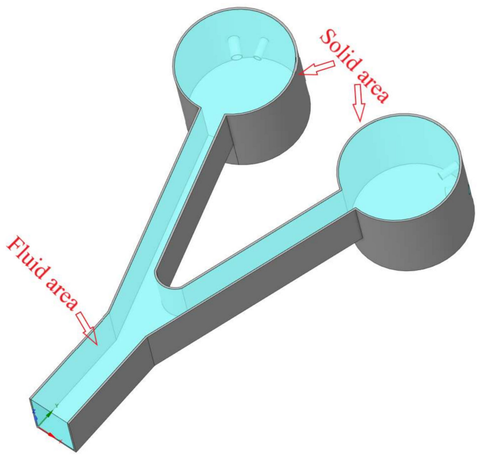

Figure 4. Solid and fluid regions.

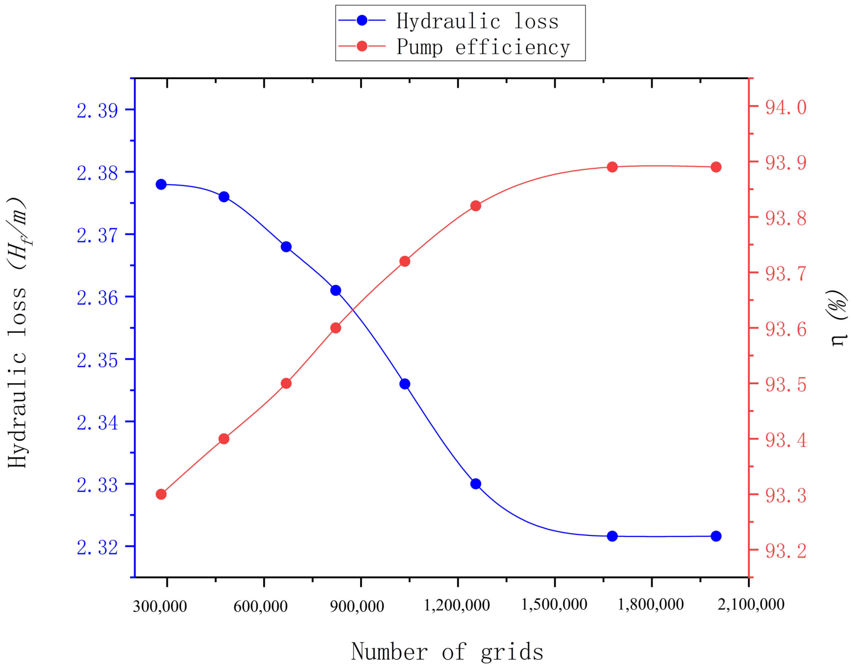

Figure 5. Hydraulic losses in the circular forebay with different grid numbers.

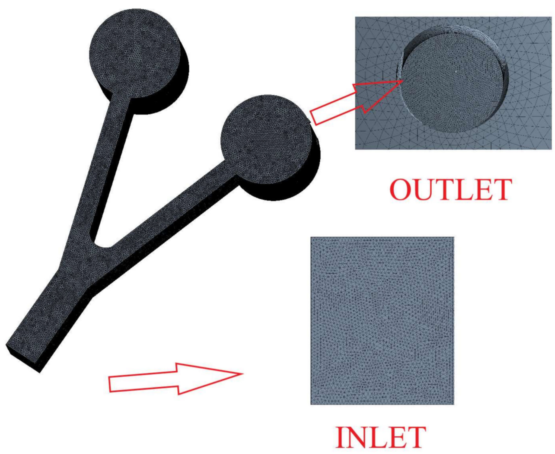

Figure 6. Mesh generation.

2.3.3. Boundary Conditions

To ensure the precision of the front pool model, we implemented the ensuing boundary conditions and corrective measures. Primarily, we employed the velocity inlet as the boundary condition for the entrance section of the forebay. This selection are based on an extensive dataset, which facilitates the determination of the inlet flow velocity and affords meticulous control over its specific flow rate. Accounting for the division of the computational domain into three distinct segments, with no consideration of the upstream region's influence on water flow in the forebay, we designated the circular forebay outlet boundary as the "outflow". Specific values were assigned based on the pumping power of the four pumps. To rectify the impact of the wall area, we employed the wall function method [36] to make the necessary adjustments. Furthermore, we designated a nonslip point of contact between the wall boundary and water flow. Additionally, the wall roughness was set at 0.005 m. For the upper boundary, we utilized the steel cover assumption method [37]. This decision accounts for the region's limited rainfall and minimal surface fluctuations, given that external factors have a relatively minor influence on water and sediment flow dynamics.

3. Results

3.1. Working Condition Arrangement

A total of 7 schemes are set up for the forebay of a circular pumping station, and the relationship between different inlet flow velocities, changes in flow patterns, and sediment content in the forebay is analyzed, as shown in Table 2. The bottom of the horizontal section of the circular forebay is set to z = 0, indicating positive upwards and negative downwards. The cross-section is shown in Table 3, and the layout of the cross-section is shown in Figure 7. In combination with the second section, various parameter settings during the simulation process are shown in Table 4.

Table 2. Different working conditions and settings.

Schemes	Inlet Flow (m^3/s)	Inlet Velocity (m/s)
1	3.39	0.6
2	3.955	0.7
3	4.52	0.8
4	5.085	0.9
5	5.65	1.0
6	6.215	1.1
7	6.78	1.2

Table 3. Parameter Values for Each Section.

Section	Section Position
z1−1	$z = 1$ m
z1−2	$z = 0.5$ m
z1−3	$z = 0$ m
z1−4	$z = -1$ m

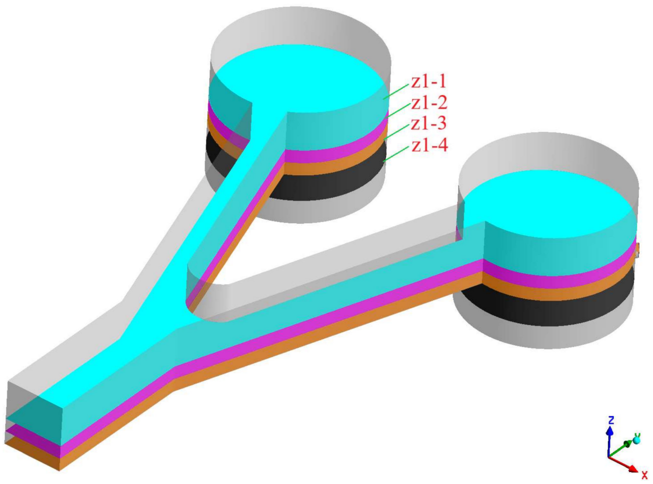

Figure 7. Cross-sectional layout.

Table 4. Simulation parameters.

Different Phases	Viscosities (kg/m·s)	Densities (kg/m^3)	Volume Fraction Ratio (%)	Time
Water	0.001	1000	99.8952	110 days
Sand	0.000103	2500	0.1048	110 days

3.1.1. Alterations in Flow Patterns among Various Schemes

As illustrated in Figure 8, the distribution of streamlines along cross-section z1−3 is presented for various schemes. From Scheme 1 to Scheme 7, it can be seen that with the escalation in initial flow velocity, alterations occur in the vortex flow configuration within the circular forebay. Within the z1−3 section, as the initial flow velocity increases, the magnitude of the vortices diminishes progressively; however, in comparison to Schemes 6 and 7, there is no considerable reduction in the vortex flow pattern. Following the ingress of inlet water, the flow velocity correspondingly diminishes upon interaction with the Y-shaped diversion pier. Upon reaching the diversion channels on both flanks, the flow velocity surges. When the initial flow velocity reaches 1.2 m/s, a substantial vortex appears after the impact in the circular forebay. As such, the numerical simulation results suggest that the flow pattern outlined in Scheme 6 is more fitting than alternative schemes.

3.1.2. Alterations in Sediment Content among Various Schemes

Figure 9 shows the sediment content distribution across cross-sections z1−3 for various schemes. Progressing from Scheme 1 to Scheme 7, a discernible pattern emerges: the sediment content in the circular forebay responds to fluctuations in the initial flow velocity. Within cross-sections z1−3, sediment content diminishes alongside the elevation in flow velocity. However, in comparison with Schemes 6 and 7, the sediment content intensifies with the surge in flow velocity. Among the array of schemes, zones characterized by elevated sediment content predominantly cluster on both flanks of the Y-shaped diversion channel sidewall. This positioning renders these areas susceptible to sediment buildup, leading to consequent interruptions to the flow pattern within the circular forebay. In stark contrast, Scheme 6 displays distinct behavior. When the initial flow velocity reaches 1.1 m/s, Scheme 6 exhibits a peak sediment content of 3.082 kg/m^3, encompassing a relatively limited expanse of high sediment concentration. As a result, it can be inferred that Scheme 6 exhibits notably diminished sediment content, consequently translating into a commensurate reduction in the potential for sediment deposition.

3.2. Parameter Verification for Each Scheme

3.2.1. Flow Velocity, Uniformity, and Deviation Angle

To verify the accuracy of the Scheme 6 results, the flow velocity uniformity v_a and deviation angle θ were introduced as reference values to calculate and demonstrate the cross-sections z1−3 of each scheme. The calculation formulas [38] for v_a and θ are:

$$v_a = \left[1 - \frac{1}{\overline{u}_a}\sqrt{\frac{\sum(u_{ai} - \overline{u}_a)^2}{m}}\right] \times 100\% \quad (9)$$

$$\theta = \frac{\sum u_{ai}\left(\tan^{-1}\frac{u_{ti}}{u_{ai}}\right)}{\sum u_{ai}} \quad (10)$$

In the formula, m represents the number of calculation units, and the number of units in z1−3 can be calculated based on the results of grid division; $\overline{u}_a$ is the average axial velocity, which can be calculated during the simulation process by setting the average axial velocity of cross-section z1−3. In cross-section z1−3, u_{ai} is the axial velocity of the i-th calculation unit, and u_{ti} is the lateral velocity of the i-th calculation unit. After calculation, the results are shown in Table 5.

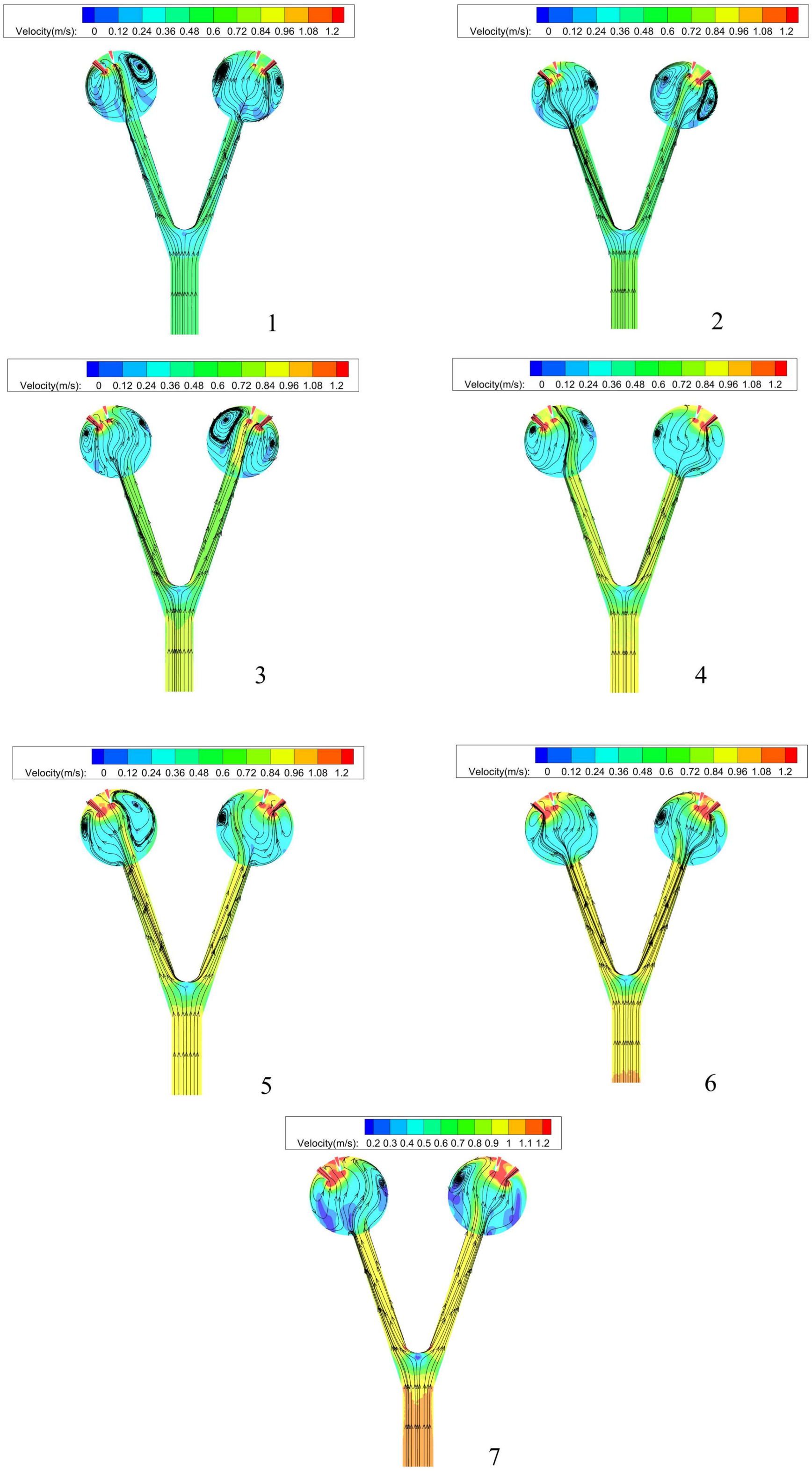

Figure 8. Flow pattern distribution of each Scheme.

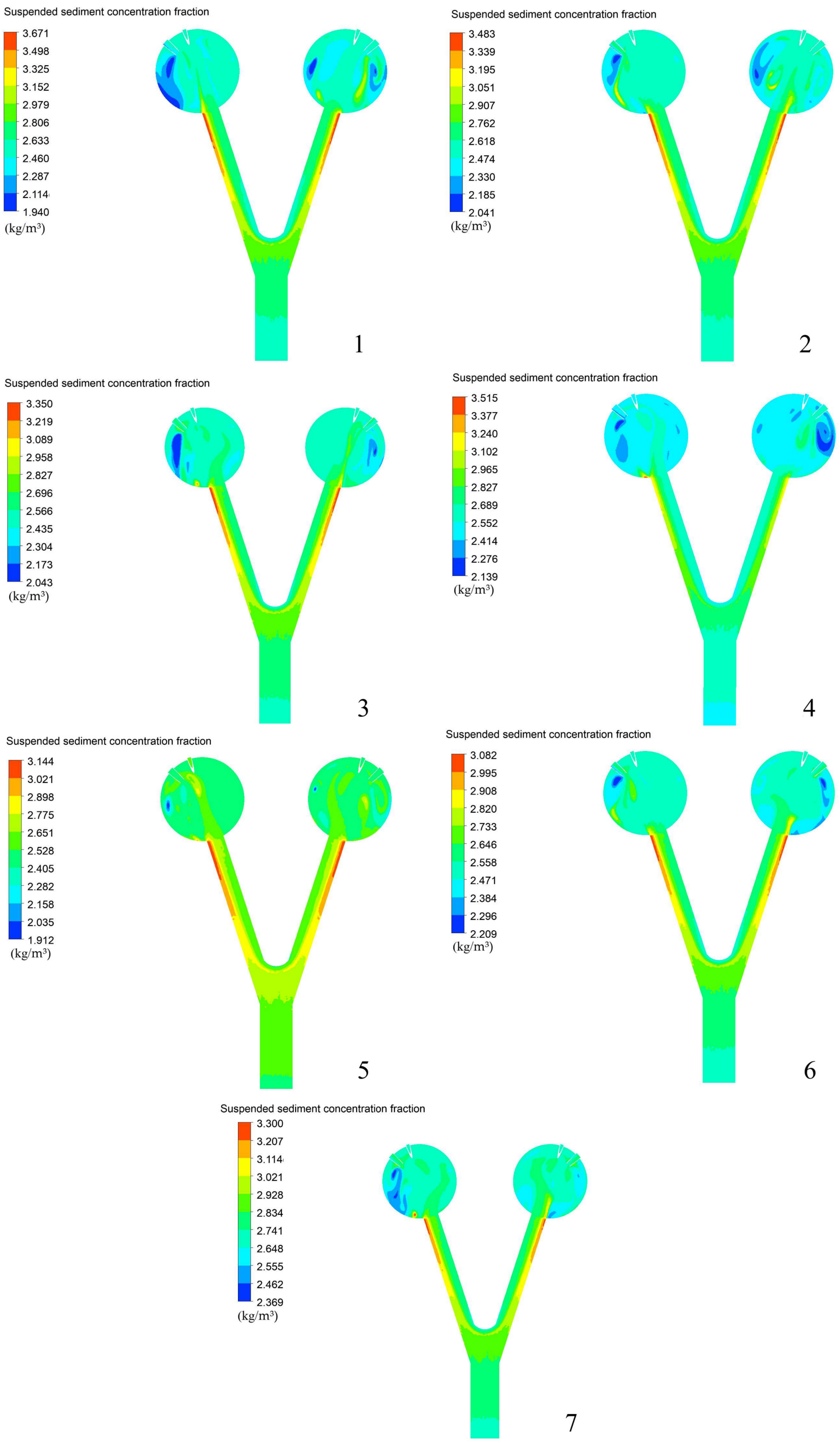

Figure 9. Sediment content distribution for each Scheme.

Table 5. Calculated values of flow velocity uniformity and deviation angle for sections z1−3.

Schemes	Observation Sections	v_a (%)	θ (°)
1	$z1-3$	84.63	20.12
2	$z1-3$	85.89	19.87
3	$z1-3$	86.15	18.94
4	$z1-3$	87.22	17.56
5	$z1-3$	87.68	16.81
6	$z1-3$	89.45	15.43
7	$z1-3$	87.31	16.95

3.2.2. Vortex Reduction Estimation

To further verify the accuracy of Scheme 6, vortex reduction estimation was introduced to calculate and analyze the vortex area. According to the formula [39]:

$$w_i = \frac{s_{wi}}{s_f} \times 100\% \tag{11}$$

$$\Delta w_i = \frac{s_{w1} - s_{wi}}{s_{w1}} \times 100\% \tag{12}$$

In the equation, w is defined in Equation (11) as the ratio of vortex area parameters, and s_{wi} is the vortex region generated by the z1−3 cross-section, as there are a total of 7 schemes, where i is taken as 1, 2, 3, 4, 5, 6, and 7. The circular area of cross-section z1−3 is set to s_f. Δw_i in Equation (12) is defined as the reduction rate of the vortex area, and the vortex area of Scheme 1 is set to s_{w1}. To verify the accuracy of each scheme, the ratio of vortex area parameters and the reduction rate of the vortex area in each scheme are calculated, as shown in Table 6.

Table 6. Vortex reduction estimates for sections z1−3.

Schemes	Vortex Area s_{wi} (m^2)	Circular Forebay Area (m^2)	Vortex Area Parameter Ratio w_i (%)	Reduction Rate Δw_i (%)
1	19.815	26.421	74.99	-
2	19.031	26.421	72.03	3.96
3	17.967	26.421	68.01	9.33
4	16.586	26.421	62.78	16.30
5	15.421	26.421	58.37	22.18
6	12.352	26.421	46.75	37.66
7	15.953	26.421	60.38	19.49

4. Discussion

4.1. Analysis of Flow Patterns in Different Schemes

From Scheme 1 to Scheme 7, different degrees of vortices will be generated. The fundamental reason for the generation of vortices is that after the mainstream water flows into the diversion channel and reaches the vicinity of Point A, a diversion phenomenon occurs, and the flow velocity decreases to a certain extent. When the diversion channel narrows after this diversion, the flow velocity will increase to a certain extent. After reaching the circular forebay, due to the high flow rate, the water flow collides with the pump outlet wall, causing rebound force and vortex generation, which affects the operation of the pumping pump in the circular forebay.

In Schemes 1 to 7, the initial flow velocity gradually increases. Lower initial flow velocities may not be sufficient to form stable vortices, but diversion through the Y-shaped diversion channel will increase the flow velocity to varying degrees, and higher flow velocities may lead to the formation of excessively strong vortices. Therefore, the flow velocity of each scheme entering the circular forebay was analyzed, as shown in Figure 10.

The dissipation rate of turbulent energy is a parameter that describes the intensity of turbulence. However, when Scheme 6 enters the forebay, the flow velocity is between 0.71 m/s and 0.98 m/s, which is much higher than other schemes in terms of the velocity change rate, resulting in a relatively increased turbulent energy dissipation rate. A higher turbulent energy dissipation rate can cause the vortex to dissipate faster after hitting the wall, thereby reducing the vortex range and making the formation and diffusion of the vortex relatively stable and localized.

In summary, Scheme 6 formed a smaller and more stable vortex structure under the condition of a moderate increase in the initial flow velocity. This flow advantage makes Scheme 6 more optimized compared to the other schemes, which is beneficial for the efficient and sustainable operation of the pumping station.

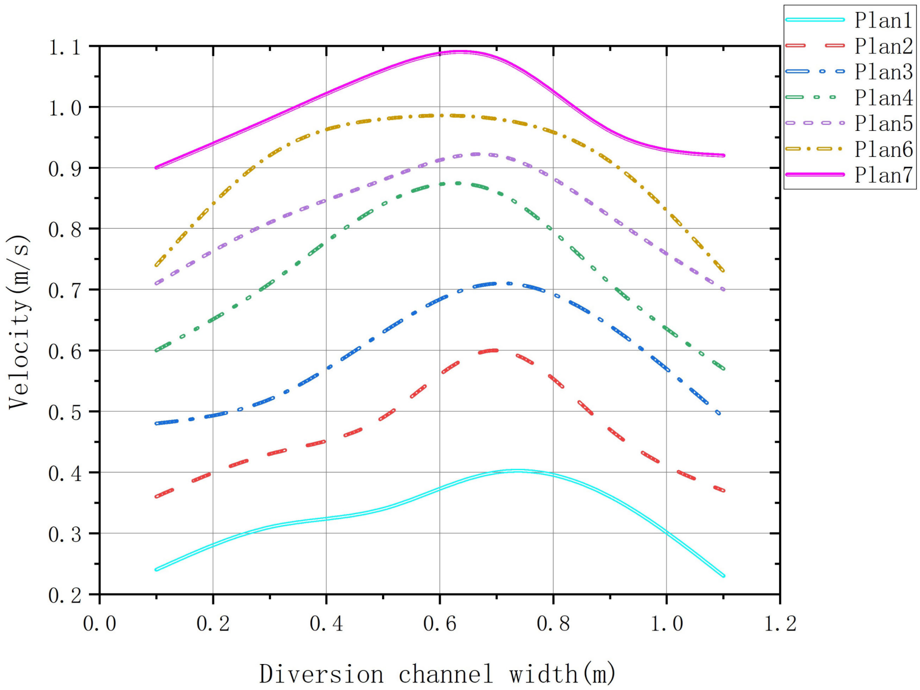

Figure 10. Comparison of flow velocity before entering the circular forebay.

4.2. Analysis of Sediment Content in Different Schemes

Because the water supply to this circular forebay originates from the Yellow River Basin and carries a substantial sediment load, there exists a strong connection between unfavorable flow patterns and sediment accumulation. Within turbulent fluid motion, the presence of vortices is frequent, and they are also generated by rotational flow. The dimensions and shapes of these vortices can significantly influence the movement and sedimentation of particles within the aquatic environment.

In the movement of mixed water-sediment flows, sediment behavior can be categorized into two main states:

1. Suspended Sediment: When encountering larger or unstable vortex flows, sediment in the water becomes suspended as a result of turbulence. These suspended particles tend to fluctuate with the movement of vortices. Higher vortex velocities hinder sediment settling in the bottom areas, decreasing the likelihood of sediment accumulation. In such cases, sediment is usually carried away with pumping action, although high sediment loads may lead to pump inlet blockage.
2. Localized Sediment Deposition: Smaller and more stable vortex flows can lead to sediment deposition in specific areas, creating concentrated sediment accumulation zones. This situation is significantly influenced by flow velocity and patterns. For instance, even though there might not be vortex zones along the sidewalls, the flow speed of

the mixed flow is lower than the sediment-carrying velocity. Consequently, sediment tends to accumulate extensively along the sidewalls of the Y-shaped diversion piers. This has a substantial impact on the main flow trajectory.

Upon reviewing Schemes 1 through 7, it becomes apparent that the sediment content within the circular forebay remains relatively low, whereas higher sediment concentrations occur along the sidewalls of the intake channel adjacent to the circular forebay. This phenomenon is primarily attributed to the fact that the primary flow generates a counterflow upon impact with the rear wall section of the circular forebay. This counterflow, in turn, creates a reactive force that circulates and rebounds the water-sediment mixture flow entering the circular forebay, further leading to an elevated sediment content near the intake channel of the circular forebay. The heightened sediment content along the sidewalls of the intake channel is primarily influenced by the impact of the water flow against the sidewalls, which results in the dissipation of kinetic energy in the mixed flow. Coupled with the friction from the sidewalls and the cumulative effect of the previously generated reactive force, this leads to the highest sediment concentration at the sidewalls of the intake channel.

In conclusion, through comparisons with the other schemes, Scheme 6 exhibits a maximum sediment content of only 3.082 kg/m^3, with a relatively limited extent of high sediment concentration zones. The lower sediment content in this scheme can be attributed to the formation of smaller yet more stable vortex structures, localized vortex diffusion, and well-regulated variations in flow velocity. The combined effects of these factors serve to mitigate the sediment content near the circular forebay and its sidewalls.

4.3. Integrated Analysis of the Optimal Scheme Based on Flow Velocity Uniformity, Deviation Angle, and Vortex Reduction Estimation

4.3.1. Analysis of Flow Velocity, Uniformity, and Deviation Angle

Flow velocity uniformity serves as a vital indicator for evaluating both the stability and uniformity of a flow field. A higher numerical value indicates a more stable flow pattern within the field. Comparing the computed values from Scheme 1 to Scheme 7, Scheme 6 stands out with a flow velocity uniformity reaching 89.45%. The significance of this lies in the fact that higher flow velocity uniformity can mitigate the erosive impact of water flow, thereby reducing sediment suspension and transport. This reduction in sediment movement contributes to lowering the potential for sediment accumulation. Moreover, a stable and uniform flow field facilitates the transportation of sediment, minimizing the likelihood of sediment deposition within the reservoir.

The deviation angle serves as an indicator of the centripetal nature of the flow velocity. A smaller resultant value suggests that the water flow tends in a horizontal direction, implying a more stable flow pattern. Scheme 6 exhibits a deviation angle of 15.43°, the lowest among all schemes. This characteristic allows Scheme 6 to more effectively diminish the rotational and swirling motion of the water flow, consequently reducing the generation and maintenance of vortices. This, in turn, contributes to a reduction in energy losses caused by vortices, leading to decreased sediment retention time and an enhancement in the operational efficiency of the pumping station.

4.3.2. Analysis of the Vortex Reduction Area Parameter Ratio and Vortex Area Reduction Rate

The vortex reduction area parameter ratio indicates the extent of vortex energy loss, with lower values indicating lower energy losses. In Scheme 6, the vortex reduction area parameter ratio is 46.75%, implying a relatively stable vortex intensity compared to other schemes. Additionally, the lower vortex reduction area parameter ratio favors vortex sustainability, enhancing the effectiveness of carrying sediment within the mixed flow by the vortices generated at this intensity during pump operation.

The vortex area reduction rate serves as a parameter for comparison with Scheme 1, revealing that Scheme 6 exhibits the highest reduction rate in the vortex area. This indicates the swift attenuation and dissipation of vortex flow within the circular forebay. The substantial reduction in vortex area leads to a relatively stable and localized vortex flow in specific areas, diminishing its range of influence across the entire forebay. Consequently, this mitigates sediment content and deposition, thereby enhancing the operational efficiency of the pumping station.

In summary, Scheme 6 outperforms the other schemes in terms of flow velocity uniformity, deviation angle, vortex area reduction ratio, and vortex area reduction rate. These attributes enable Scheme 6 to more effectively reduce sediment content and deposition, optimizing the flow patterns within the circular forebay. This enhancement contributes to the elevated operational efficiency of the pumping station and decreased maintenance costs.

4.4. Experimental Verification

From June to September 2022, field experiments were conducted to validate Scheme 6. By adjusting the inlet valve, the initial flow velocity was set according to Scheme 6. The following parameters were then verified:

4.4.1. Flow Velocity Verification

In the experiment, a total of 13 streamline measurement points were set up, and their distribution is shown in Figure 11. The spacing between adjacent measurement points on each streamline is 0.5 m, and the spacing between lines A, B, and C is 0.3 m. The spacing between lines L1, L2, and L3 is 1 m, and the spacing between lines C and D is 0.2 m. The depth of the flow velocity measurement in the diversion channel is 2 m, and the depth of the flow velocity measurement in the forebay is 3 m. By comparing the measured flow velocity data with the numerical simulation, the comparison results are shown in Figure 12. The error between the measured data and the numerical simulation results is extremely small, and their changing trends are almost identical. The accuracy of Scheme 6 was once again verified, which correspondingly improved the sustainability of the circular pumping station project.

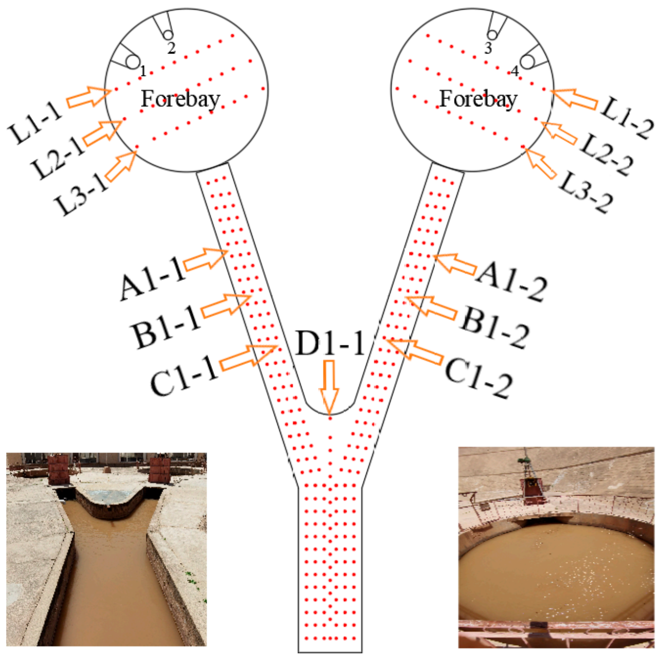

Figure 11. Layout of the measuring points in the circular forebay.

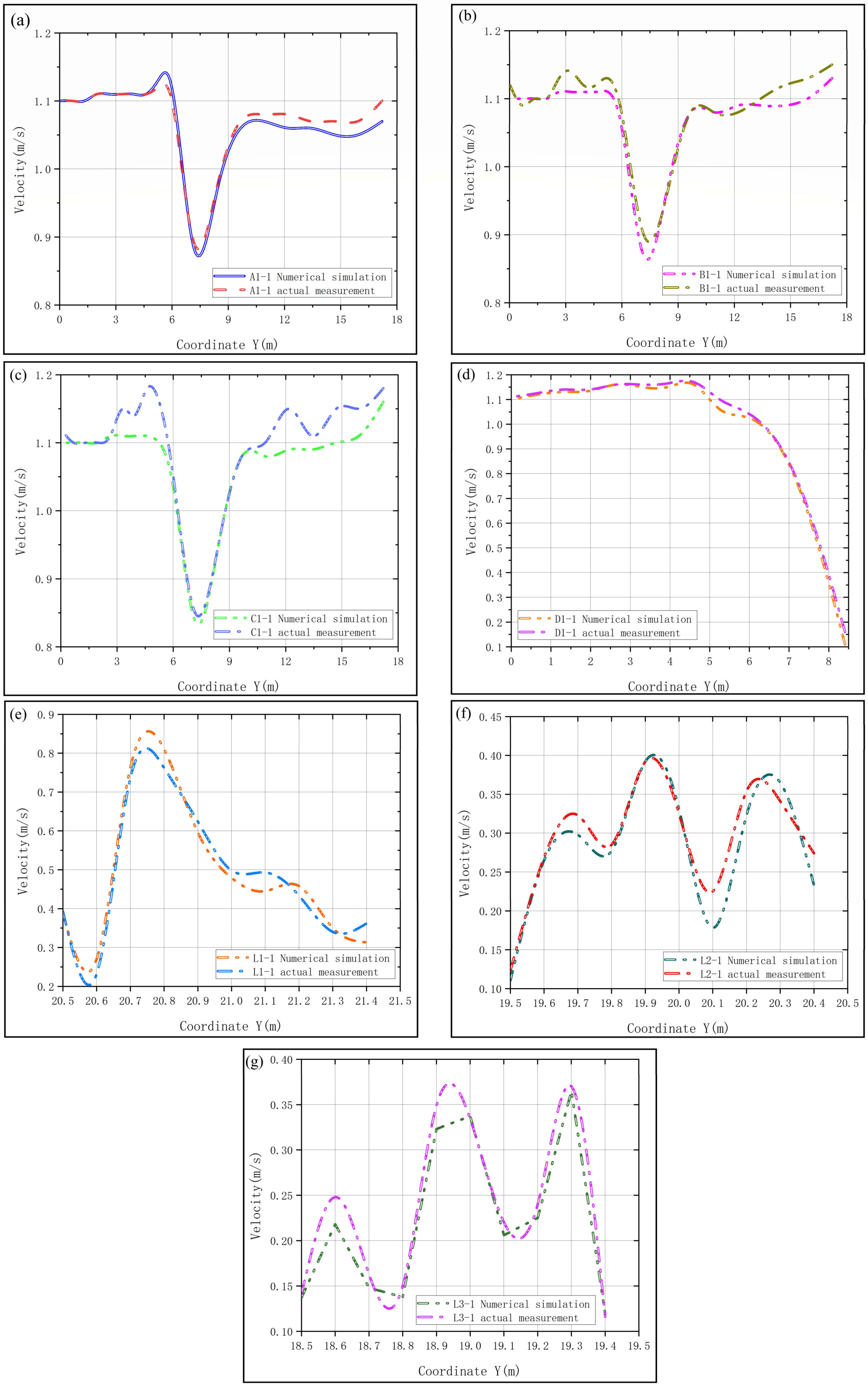

Figure 12. Comparison of Flow Velocities in Different Lines: (**a**) A1-1 Velocities Comparison. (**b**) B1-1 Velocities Comparison. (**c**) C1-1 Velocities Comparison. (**d**) D1-1 Velocities Comparison. (**e**) L1-1 Velocities Comparison. (**f**) L2-1 Velocities Comparison. (**g**) L3-1 Velocities Comparison.

4.4.2. Sediment Accumulation Verification

In the period from June to September 2022, following the completion of pump station operation based on Scheme 6, sediment accumulation was measured. Comparing the sediment accumulation status in the forebay from June to September 2021, the thickness variations are presented in Figure 13. The maximum reduction in thickness reached 0.67 m, and there was an overall decrease in sediment accumulation within the intake channel. This once again validates the rationality of Scheme 6.

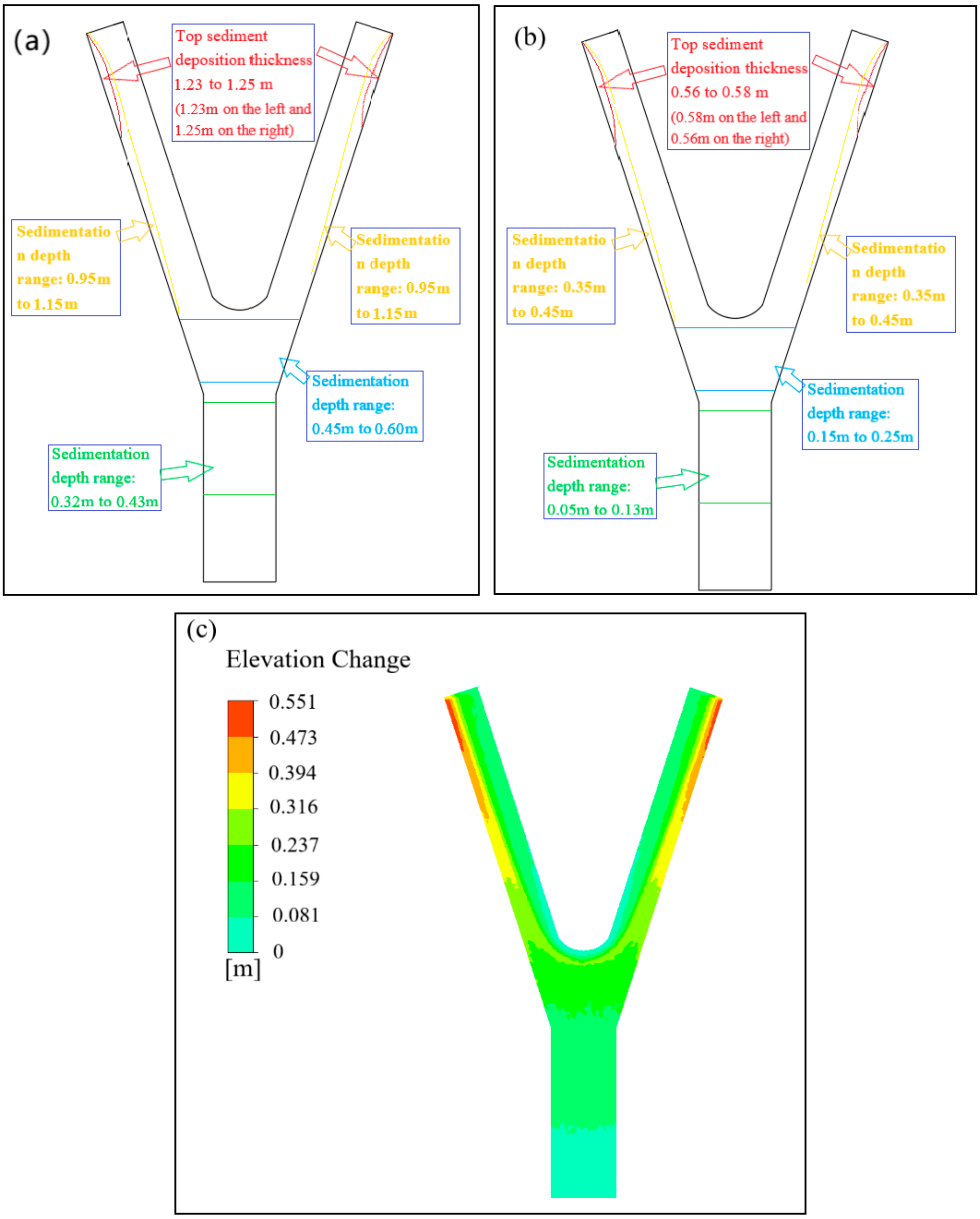

Figure 13. Sediment accumulation comparison chart. (**a**) Sediment accumulation in 2021; (**b**) Sediment accumulation in 2022; (**c**) Elevation variation in the scheme 6 numerical simulation.

5. Conclusions

This research focuses on the numerical simulation of water and sediment two-phase flow under various operating conditions in the forebay of a circular pumping station in Gansu Province, aiming to improve the sustainability of the forebay of the circular pumping station. The main conclusions are as follows:

(1) Using numerical simulation to calculate the flow patterns in different turbulence models and comparing the calculation results with multiple engineering measurements to confirm that the standard $k-\varepsilon$ model conforms to actual operating conditions.
(2) Through theoretical analysis of simulation results of different flow velocities of water and sediment two-phase flow, it can be concluded that the flow state of the diversion channel is relatively stable, but there will be obvious vortices generated in the forebay, and there will be varying degrees of sediment accumulation in the diversion channel and forebay.
(3) The flow pattern in the forebay will change to varying degrees with the flow velocity. From Scheme 1 to Scheme 6, as the flow velocity increases, the optimization performance of the flow pattern gradually improves, and the sediment content also shows a decreasing state. However, when the flow velocity is increased again in Scheme 7, the flow pattern further deteriorates, and the sediment content also increases.
(4) At the initial flow rate of Scheme 6, the uniformity of the flow rate is improved by 4.82% compared to Scheme 1, and the deviation angle is reduced by 4.69°. The parameter ratio of the vortex reduction area and the reduction rate of the vortex area have been significantly optimized. Therefore, condition 6 is the optimal initial flow rate.
(5) After adopting Scheme 6 for operation in the project, the actual flow velocity in the forebay was basically consistent with the numerical simulation results. The sediment deposition had a significant reduction effect compared to the previous year, and the sediment deposition thickness was reduced to its maximum extent by 0.67 m.

By combining numerical simulation, theoretical analysis, and practical engineering projects, the causes of vortex and sediment accumulation in the circular forebay are analyzed. The optimal working conditions for the circular forebay under different working conditions are proposed. At the same time, the sustainability of different working conditions is verified by combining parameters such as the average flow velocity uniformity, deviation angle, vortex area parameter ratio, and vortex area reduction rate. This provides theoretical support for the working conditions and renovation of the circular forebay in the future.

Author Contributions: Methodology, H.W. and Y.T.; software, H.W., Y.T. and H.J.; validation, H.W., Y.T., L.H. and C.Y.; formal analysis, H.W., L.H. and C.Y.; investigation, H.W., L.H. and H.J.; resources, H.W. and L.H.; data curation, H.W. and Y.T.; writing—original draft, H.W.; writing—review & editing, H.W. and L.H.; supervision, H.W. All authors have read and agreed to the published version of the manuscript.

Funding: This work was supported by the Natural Science Foundation of Ningxia Province (Grant No. 2023AAC02049 and Grant No. 2021AAC03096) and the Natural Science Foundation of China (Grant No. 11761005).

Data Availability Statement: The data that supports the findings of this study are available from the corresponding author upon reasonable request.

Conflicts of Interest: The authors declare that they have no known competing financial interest or personal relationships that could influence the work reported in this paper.

References

1. Yonghai, Y.; Haodi, Y.; Changliang, Y. Parameter optimization of rectification sill in the forebay of pumping station using BPNN-GA algorithm. *Trans. Chin. Soc. Agric. Eng.* **2023**, *39*, 106–113.
2. Zhang, Y. Study on Hydraulic Characteristics of Forebay and Sump of Large Pumping Station. Master's Thesis, Xi'an University of Technology, Xi'an, China, 2022. (In Chinese).
3. Xinjian, F.; Chunhai, D.; Zhijun, W.; Ya'Nan, L.; Wei, Y. Influence of diffusion angle on flow field structure in forward intake forebay of pumping station. *Trans. Chin. Soc. Agric. Eng.* **2023**, *39*, 92–99.
4. Ming, L.; Yong, W.; Wei, X.; Xiaolin, W.; Houlin, L. Optimizing the geometric parameters for the lateral inflow forebay of the pump sump. *Trans. Chin. Soc. Agric. Eng.* **2022**, *38*, 69–77.
5. Zhang, C.; Yan, H.; Jamil, M.T.; Yu, Y. Improvement of the Flow Pattern of a Forebay with a Side-Intake Pumping Station by Diversion Piers Based on Orthogonal Test Method. *Water* **2022**, *14*, 2663. [CrossRef]
6. Wang, H.; Li, C.; Lu, S.; Song, L. The flow patterns and sediment deposition in the forebay of a forward-intake pumping station. *Phys. Fluids* **2022**, *34*, 083316. [CrossRef]
7. Fujun, W.; Xuelin, T.; Xin, C.; Ruofu, X.; Zhifeng, Y.; Wei, Y. A review on flow analysis method for pumping stations. *J. Hydraul. Eng.* **2018**, *49*, 47–61.
8. Li, Y.; Gu, J.; Guo, C.; Zhou, C. Flow Patterns and Rectification Measures in the Forebay of Pumping Station. *IOP Conf. Ser. Mater. Sci. Eng.* **2020**, *794*, 12058. [CrossRef]
9. Zhan, J.M.; Wang, B.C.; Yu, L.H.; Li, Y.S.; Ling, T. Numerical investigation of flow patterns in different pump intake systems. *J. Hydrodyn.* **2012**, *24*, 873–882. [CrossRef]
10. Hui, F.; Huasi, N.; Yujia, M.; Ruobing, Y.; Xinlei, G.; Chunrong, S. Hydraulic performance optimization of the ultra narrow union pumping forebay: A case study. *J. Hydraul. Eng.* **2020**, *51*, 788–795.
11. Can, L.; Shuaihao, L.; Yao, Y.; Li, C.; Du, K. Numerical simulation research on inlet flow pattern of small sluice station lateral pumping station. *J. Drain. Irrig. Mach. Eng.* **2021**, *39*, 797–803.
12. Xu, C.; Wang, R.; Liu, H.; Zhang, R.; Wang, M.; Wang, Y. Flow pattern and anti-silt measures of straight-edge forebay in large pump stations. *Int. J. Heat Technol.* **2018**, *36*, 1130–1139. [CrossRef]
13. Caishui, H. Three-dimensional Numerical Analysis of Flow Pattern in Pressure Forebay of Hydropower Station. *Procedia Eng.* **2012**, *28*, 128–135. [CrossRef]
14. Nasr, A.; Yang, F.; Zhang, Y.; Wang, T.; Hassan, M. Analysis of the Flow Pattern and Flow Rectification Measures of the Side-Intake Forebay in a Multi-Unit Pumping Station. *Water* **2021**, *13*, 2025. [CrossRef]
15. Xi, W.; Lu, W.G. Formation Mechanism of an Adherent Vortex in the Side Pump Sump of a Pumping Station. *Int. J. Simul. Model.* **2021**, *20*, 327–338. [CrossRef]
16. Tang, X.; Wang, W.; Wang, F.; Yu, X.; Chen, Z.; Shi, X. Application of LBM-SGS Model to Flows in a Pumping-Station Forebay. *J. Hydrodyn.* **2010**, *22*, 196–206. [CrossRef]
17. Xu, W.; Cheng, L.; Du, K.; Yu, L.; Ge, Y.; Zhang, J. Numerical and Experimental Research on Rectification Measures for a Contraction Diversion Pier in a Pumping Station. *J. Mar. Sci. Eng.* **2022**, *10*, 1437. [CrossRef]
18. Lyons, M.; Simmons, S.; Fisher, M.; Williams, J.S.; Lubitz, W.D. Experimental Investigation of Archimedes Screw Pump. *J. Hydraul. Eng.* **2020**, *146*, 4020057. [CrossRef]
19. Parsons, A.J.; Bracken, L.; Poeppl, R.E.; Wainwright, J.; Keesstra, S.D. Introduction to special issue on connectivity in water and sediment dynamics. *Earth Surf. Proc. Land* **2015**, *40*, 1275–1277. [CrossRef]
20. Budinski, L.; Spasojević, M. 2D Modeling of Flow and Sediment Interaction: Sediment Mixtures. *J. Waterw. Port Coast. Ocean Eng.* **2014**, *140*, 199–209. [CrossRef]
21. Serra, T.; Soler, M.; Barcelona, A.; Colomer, J. Suspended sediment transport and deposition in sediment-replenished artificial floods in Mediterranean rivers. *J. Hydrol.* **2022**, *609*, 127756. [CrossRef]
22. Yuan, Q.; Zhang, M.; Zhou, J. To Implement A Clear-Water Supply System for Fine-Sediment Experiment in Laboratories. *Water* **2019**, *11*, 2476. [CrossRef]
23. Mirmasoumi, S.; Behzadmehr, A. Numerical study of laminar mixed convection of a nanofluid in a horizontal tube using two-phase mixture model. *Appl. Therm. Eng.* **2008**, *28*, 717–727. [CrossRef]
24. Li, J.N.; Chen, X.H. A multi-dimensional two-phase mixture model for intense sediment transport in sheet flow and around pipeline. *Phys. Fluids* **2022**, *34*, 103314. [CrossRef]
25. Onishi, T.; Peng, Y.; Ji, H.; Peng, G. Numerical simulations of cavitating water jet by an improved cavitation model of compressible mixture flow with an emphasis on phase change effects. *Phys. Fluids* **2023**, *35*, 73333. [CrossRef]
26. Almeland, S.K.; Olsen, N.R.B.; Bråveit, K.; Aryal, P.R. Multiple solutions of the Navier-Stokes equations computing water flow in sand traps. *Eng. Appl. Comp. Fluid* **2019**, *13*, 199–219. [CrossRef]
27. Ozmen-Cagatay, H.; Kocaman, S. Dam-Break Flow in the Presence of Obstacle: Experiment and CFD Simulation. *Eng. Appl. Comp. Fluid* **2011**, *5*, 541–552. [CrossRef]
28. Ghai, S.K.; Ahmed, U.; Klein, M.; Chakraborty, N. Turbulent kinetic energy evolution in turbulent boundary layers during head-on interaction of premixed flames with inert walls for different thermal boundary conditions. *Proc. Combust. Inst.* **2023**, *39*, 2169–2178. [CrossRef]

29. Zhao, L.; Liu, D.; Lin, J.; Chen, L.; Chen, S.; Wang, G. Estimation of turbulent dissipation rates and its implications for the particle-bubble interactions in flotation. *Miner. Eng.* **2023**, *201*, 108230. [CrossRef]
30. Cheng, Y.; Lien, F.S.; Yee, E.; Sinclair, R. A comparison of large Eddy simulations with a standard k–ε Reynolds-averaged Navier–Stokes model for the prediction of a fully developed turbulent flow over a matrix of cubes. *J. Wind. Eng. Ind. Aerodyn.* **2003**, *91*, 1301–1328. [CrossRef]
31. Ahn, S.; Xiao, Y.; Wang, Z.; Luo, Y.; Fan, H. Unsteady prediction of cavitating flow around a three dimensional hydrofoil by using a modified RNG k-ε model. *Ocean Eng.* **2018**, *158*, 275–285. [CrossRef]
32. Moen, A.; Mauri, L.; Narasimhamurthy, V.D. Comparison of k-ε models in gaseous release and dispersion simulations using the CFD code FLACS. *Process. Saf. Environ.* **2019**, *130*, 306–316. [CrossRef]
33. Oosterkamp, A.; Ytrehus, T.; Galtung, S.T. Effect of the choice of boundary conditions on modelling ambient to soil heat transfer near a buried pipeline. *Appl. Therm. Eng.* **2016**, *100*, 367–377. [CrossRef]
34. Folkner, D.; Katz, A.; Sankaran, V. Design and verification methodology of boundary conditions for finite volume schemes. *Comput. Fluids* **2014**, *96*, 264–275. [CrossRef]
35. Sojoudi, A.; Nourbakhsh, A.; Shokouhmand, H. Establishing a Relationship between Hydraulic Efficiency and Temperature Rise in Centrifugal Pumps: Experimental Study. *J. Hydraul. Eng.* **2018**, *144*, 4018011. [CrossRef]
36. Hadžiabdić, M.; Ničeno, B. Reconstruction of Nusselt number in RANS computations with wall function approach. *Nucl. Eng. Des.* **2023**, *412*, 112461. [CrossRef]
37. Wang, H.; Li, C.; Lu, S.; Yang, C.; Huang, L. Numerical and experimental study on vortex optimization in the forebay of a Sandy River. *Phys. Fluids* **2023**, *35*, 085128. [CrossRef]
38. Zi, D.; Wang, F.; Yao, Z.; Hou, Y.; Xiao, R.; He, C.; Yang, E. Effects analysis on rectifying intake flow field for large scale pumping station with combined diversion piers. *Trans. Chin. Soc. Agric. Eng.* **2015**, *31*, 71–77.
39. Yang, F.; Zhang, Y.; Liu, C.; Wang, T.; Jiang, D.; Jin, Y. Numerical and Experimental Investigations of Flow Pattern and Anti-Vortex Measures of Forebay in a Multi-Unit Pumping Station. *Water* **2021**, *13*, 935. [CrossRef]

Disclaimer/Publisher's Note: The statements, opinions and data contained in all publications are solely those of the individual author(s) and contributor(s) and not of MDPI and/or the editor(s). MDPI and/or the editor(s) disclaim responsibility for any injury to people or property resulting from any ideas, methods, instructions or products referred to in the content.